"Peak tracking chip" for label-free optical detection of bio-molecular interaction and bulk sensing

Kristelle Bougot-Robin, Shunbo Li, Yinghua Zhang, I-Ming Hsing, Henri Benisty, Weija Wen

"Peak tracking chip" for label-free optical detection of bio-molecular interaction and bulk sensing

Kristelle Bougot-Robin,[a] Shunbo Li,[b] Yinghua Zhang,[c] I-Ming Hsing,[c] Henri Benisty[d] and Weijia Wen*[b]

A novel imaging method for bulk refractive index sensing or label-free bio-molecular interaction sensing is presented. This method is based on specially designed "Peak tracking chip" (PTC) involving "tracks" of adjacent resonant waveguide gratings (RWG) "micropads" with slowly evolving resonance position. Using a simple camera the spatial information robustly retrieves the diffraction efficiency, which in turn transduces either the refractive index of the liquids on the tracks or the effective thickness of an immobilized biological layer. Our intrinsically multiplex chip combines tunability and versatility advantages of dielectric guided wave biochips without the need of costly hyperspectral instrumentation. The current success of surface plasmon imaging techniques suggests that our chip proposal could leverage an untapped potential to routinely extend such techniques in a convenient and sturdy optical configuration toward, for instance for large analytes detection. PTC design and fabrication are discussed with challenging process to control micropads properties by varying their period (step of 2 nm) or their duty cycle through the groove width (steps of 4 nm). Through monochromatic imaging of our PTC, we present experimental demonstration of bulk index sensing on the range [1.33–1.47] and of surface biomolecule detection of molecular weight 30 kDa in aqueous solution using different surface densities. A sensitivity of the order of 10^{-5} RIU for bulk detection and a sensitivity of the order of $\sim$10 pg mm^{-2} for label-free surface detection are expected, therefore opening a large range of application of our chip based imaging technique. Exploiting and chip design, we expect as well our chip to open new direction for multispectral studies through imaging.

Introduction

Resonant properties are frequently used to measure refractive index variation at a chip surface. Thanks to resonant light–matter interaction, detection of a small change of effective refractive index becomes feasible. Favorable applications are bulk refractive index sensing and biological interaction sensing with immobilized probes. Several strategies have been proposed for the detection of refractive index variation on a chip, as the chip format can allow sensitive detection and use of a small amount of sample. However, most demonstrations are restricted to the sensing of a limited number of analytes at a time and at a single wavelength,[1,2] with the notable exception of the more mature surface plasmon resonance imaging (SPRi).[3] Imaging offers such a high information throughput that it intrinsically lends itself to multiplex assays, with secure features such as keeping a reference signal for self-calibration purposes. Here, we generalize this idea by including a scan of the resonance within the very multiplexing scheme, leaving ample "spatial bandwidth" for bona fide biological multiplexing.

If we look into the general issue of biological sensing, measurement of different interactions in parallel opens a wide range of applications, but costly resulting instruments have led to increasing consideration of miniature approaches and thus, biochips. Biochip imaging techniques are intrinsically multiplex and hold the leading position for bioarray reading. Multiplexing is obtained by immobilizing different species at the surface of the chip, which interact with target biomolecules in solution based on their different affinities. Biochip imaging has been widely developed using fluorescence signals as these allow highly sensitive detection. However, fluorophore labeling induces costs in terms of time and of consumables; labels are also prone to photobleaching and, last but not least, they may interfere with the affinity of many biomolecules and spoil the desired information. Enhancement strategies (multilayer,[4] photonic crystal structuration,[5] or plasmon[6,7]) are often necessary to reduce the background in real-time detection applications, *e.g.*, with modestly purified samples.

[a]*Institute for Advanced studies, Hong-Kong University of Science and Technology, Clear Water Bay, Kowloon, Hong-Kong, China. E-mail: kristelle_robin@yahoo.fr*
[b]*Department of Physics, Hong-Kong University of Science and Technology, Clear Water Bay, Kowloon, Hong-Kong, China. E-mail: phwen@ust.hk*
[c]*Department of Chemical and Biomolecular Engineering, The Hong Kong University of Science and Technology, Kowloon, Hong-Kong, China*
[d]*Institut Optique Graduate School, 2 avenue Fresnel, Campus Polytechnique, 91127 Palaiseau, France*

Therefore, label-free techniques based on a transduction of refractive index variation at the chip surface have never faltered since their inception. Among label-free resonant techniques exploiting resonant conditions, SPRi mentioned above is the most widely developed technique.[8] A good alternative, that has become realistic and cheap enough thanks to maturing nano-imprinting techniques, consists of using dielectric resonant waveguide gratings (RWGs) or other 3D waveguide structures. These can allow similar sensitivity[9] and more flexibility using the richer geometry of the resonant structures, for instance to tune the vertical spatial extent of the wave and then optimize the interaction with the analyte for detection.[10] For a robust optical design enabling sturdy readers, the diffracted direction of emerging light may also be optimized for convenient wide-field imaging, *e.g.*, normal to chip surface.

SPR imaging or RWG imaging are based on the change of reflection/diffraction efficiency induced by the index change in the bulk or close to the surface, induced by bio-molecules. Such imaging involves spectral and angular filtering to probe a well identified condition around the resonance. The SPR is intrinsically less dispersive than the RWG resonance and can be used with relaxed filtering conditions. The approach of direct spectroscopic measurement has been developed with waveguide structures, using modulated lasers to scan a highly sensitive resonance.[11] Multiplex chip configurations have also been proposed on chips having multiple integrated Bragg gratings UV-written in silica waveguides[12] and probed through their guided reflection, with multiple optical fibers for coupling broad spectrum light and read-out optical spectra, thus requiring multiple optical fibers coupling with the well-known associated coupling problems. All these techniques have restricted multiplexing capabilities and/or result in delicate mounts, thus prompting a need to fully explore and exploit 2D imaging.

Recently, direct 2D RWG-imaging (one shot simple image for all spots on a microarray format) with monochromatic illumination has been shown to detect a biomolecule monolayer in dry phase (biomolecules in air without fluidic integration). This technique is thus valid for end-point detection.[13] Real-time detection with fluidic flow and with highly filtered illumination conditions brings new issues in term of background as it becomes critical to disentangle background from optical and biological origins. Therefore, the main experimental demonstrations and commercialized techniques involving dielectric RWG devices are rather based on the use of spectral information to reconstruct bi-dimensional images for spatially multiplexed detection, in spite of the longer time and much heavier treatment required to obtain a chip image in comparison with direct 2D imaging. By definition, spectra are sequences of intensity values depending on the wavelength. Using a sequence allows robust measurements, compliant against mixture of optical and biological background drifts. But the associated instrumentation implies either a so-called spectro-imager detector[14] or scanning a tunable source.[11,15] Bi-dimensional information of a 2D chip surface is generally reconstructed by analyzing the hyperspectral information, seeking for instance peak shifts towards longer wavelength to track the increase of refractive index at the chip surface. Angular scanning at a single wavelength offers an alternative solution, but its sequential nature also leads to a long reconstructing step to get the 2D chip surface measurement,[16] and to risks with drift and calibration.

It is thus desirable to find a way to exploit full 2D imaging in monochromatic illumination to render the information retrieval more robust. As hinted above, our idea is that we may use part of the large information throughput of optical images to achieve this, and more precisely to get an image equivalent to a diffraction efficiency scan around a resonance ("sequence") using a special chip design. In this paper, we propose for this purpose a new multiplex method based on a novel "peak-tracking chip" (PTC) which allows robust measurements through the use of intensity sequences.

"Peak-tracking chip" principle and applications

Peak-tracking chip design

Using an array of resonant structures of neighboring resonance condition excited at a single (λ, θ) illumination condition, our PTC exploits the spatial change across an array of such micropads from a "one-shot" bi-dimensional image. Measurements are captured by a simple commercial camera to determine the effective refractive index variation occurring at the chip surface, which is uniform across one of these arrays. Multiplexing simply comes from the capability to image many such arrays, called "tracks" below, and each of size ~0.06 Mpixels, within a single ~42 Mpixels reflected intensity image frame.

For multiplexing purpose, micropads are juxtaposed in linear arrays called "tracks", each such track becoming a sensing region as illustrated in Fig. 1(A). Multiple "tracks" are disposed on the chip in a 2D geometry fitting into the imaged frame to exploit imaging information throughput. Multiplex aspect is also a key component of self-referenced measurement, for robust (temperature, optical motion, unspecific binding drifts…) and sensitive detection.[17]

In this paper, to obtain micropads of neighboring resonant conditions, we use resonant waveguide gratings micropads of varying geometry. Through small changes in micropad parameters, for instance period, duty cycle, waveguide layer thickness, etching thickness, light can be coupled so as to sample the neighboring of the resonance peak, and therefore provide a genuine resonance scan through a monochromatic image intensity measurement.

In this work, the parameters varied between micropads of our tracks are either the grating period or its duty cycle (mark-space ratio), that is, in-plane parameters. The duty cycle case is illustrated in Fig. 1(A) for a chip with 3 × 2 tracks. Fig. 1(B) illustrates the basic optical set-up for monochromatic imaging. Fig. 1(C) gives a scheme of side-view of one of the grating micropads with period $\Lambda_0 = 450$ nm and duty cycle $f_i = 0.3$ while Fig. 1(D) gives a top view of these micropads from ×70000 SEM (scanning electron microscopy) images after photo-resist development.

"Tracks" properties

Using a scattering matrix formalism,[18,19] diffraction efficiency values of grating micropads are calculated using electromagnetic simulations initially implemented for the study of 2D photonic crystal structures.[20] The chip is optimized for detection at small incidence angle, for a green wavelength, initially to exploit the $\lambda = 546$ nm spectral line of a mercury lamp at small incidence

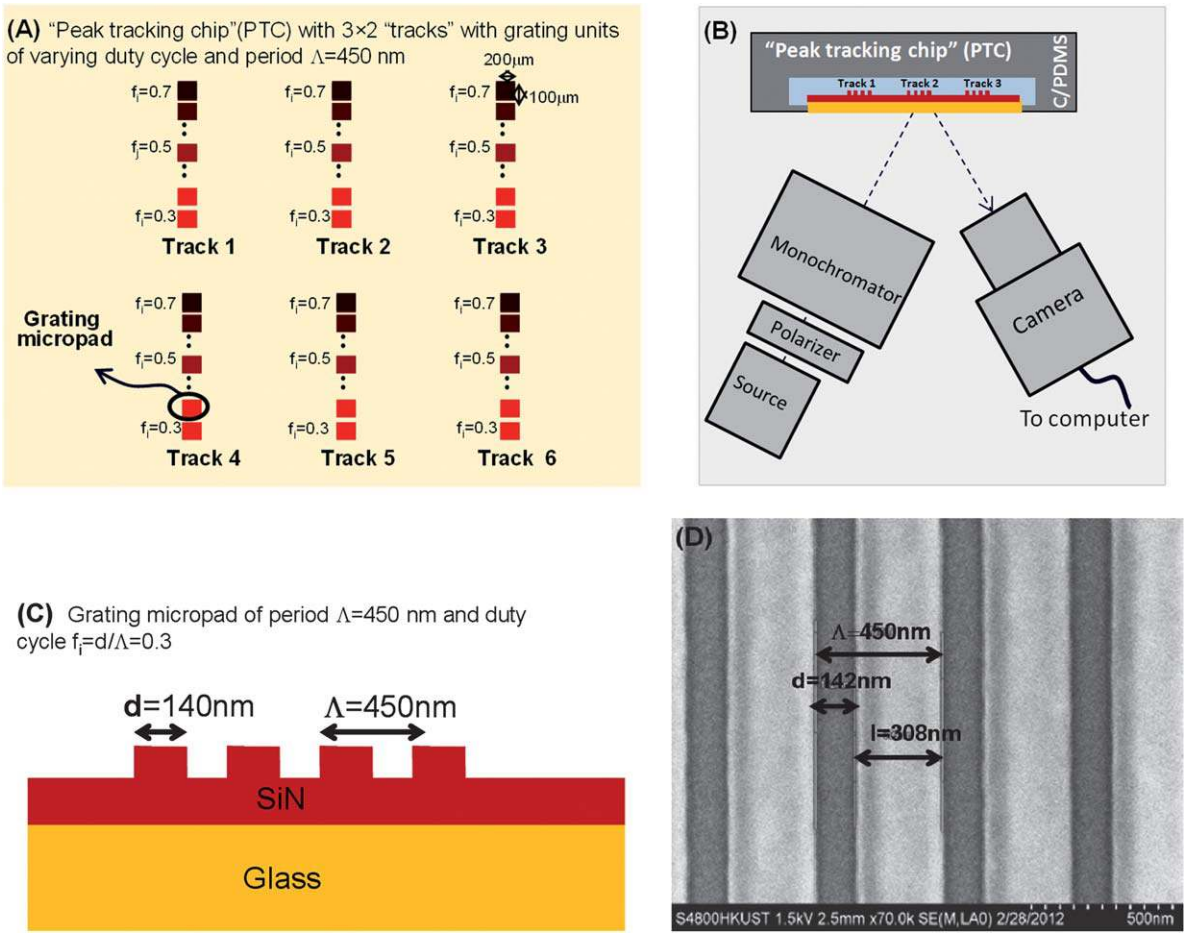

Fig. 1 (A) Top view of the chip with 3 × 2 "tracks" on its surface. Each "track" consists of grating "micropads" of identical period $\Lambda = 450$ nm and variable duty cycle f_i. Size of each "micropad" is of 200 × 100 μm^2. (B) Optical set-up used to image the "peak tracking chip" composed of a monochromatic polarized simple source illuminating the chip and measured through a camera to measure the 2D images. (C) Side view of a grating in a micropad composed of high index SiN layer on low index glass substrate. The etched grating period is Λ, the ridge width d and thus the duty cycle $f = d/\Lambda = 0.30$ with period $\Lambda = 450$ nm. (D) SEM image of the micropad sketched in (C) after photoresist development.

angle. A small angle is compatible with near-normal incidence imaging so a larger frame area can be captured within the depth of focus. For our optimization, we take into account fabricated materials parameters as well as electron-beam lithography limitations. The materials chosen for the chip are silicon nitride ($n = 2.07 + 0.003i$ from our ellipsometry measurement), and for the substrate, borosilicate glass (approximate composition 70% silica, 10% boron oxide, 8% sodium oxide, 8% potassium oxide, and 1% calcium oxide, $n \sim 1.47$ from provider specification). We choose a central period $\Lambda = 450$ nm and central duty cycle $f_0 = 0.5$. To confine the guided wave while retaining a good sensitivity to index variation of the ambient (cover) medium, we choose a silicon nitride layer thickness of 0.27Λ (122 nm) etched to a depth of 0.15Λ (67 nm). On a given track, either the period Λ_i is varied, here from 440 nm to 460 nm at a constant duty cycle $f_0 = 0.5$, or the duty cycle f_i is varied from 0.3 to 0.7 at a fixed period $\Lambda = 450$ nm. The other targeted parameters of the gratings remain unchanged (waveguide layer thickness, optical index, etching depth). The intensity scale level is adjusted to [0–0.6]. Indeed, losses in the silicon nitride layer induce a substantial decrease in peak reflectivity. The pitch between grating grooves or lines is discretized by the digitizing grid of the electron-beam (e-beam) exposure process. The pattern is realized using a JEOL JBX-6300FS e-beam system. The best precision achievable in line position is of 1 nm, and the minimum stripe groove width variation step is 4 nm.[21,22] We will see that this result is obtained, not intuitively, in a coarser sensing when varying the period rather than while varying the duty cycle.

Applications

Applications considered concern bulk refractive index detection and biomolecules sensing. For the first application, the model is a change of refractive index of the whole fluid above the chip, while for biomolecules sensing, the model assumes only an additional thin layer of refractive index $n = 1.5$ and thickness h_{DNA}. The reflected intensity of our PTC is calculated by electromagnetic simulations. In Fig. 2 we give the diffraction efficiency maps depending on micropads characteristics for monochromatic TM polarized light illumination at $\lambda = 546$ nm and incidence angle $\theta = 17°$, either (A and B) depending on bulk refractive index respectively with period variation (PV-PTC) and duty cycle

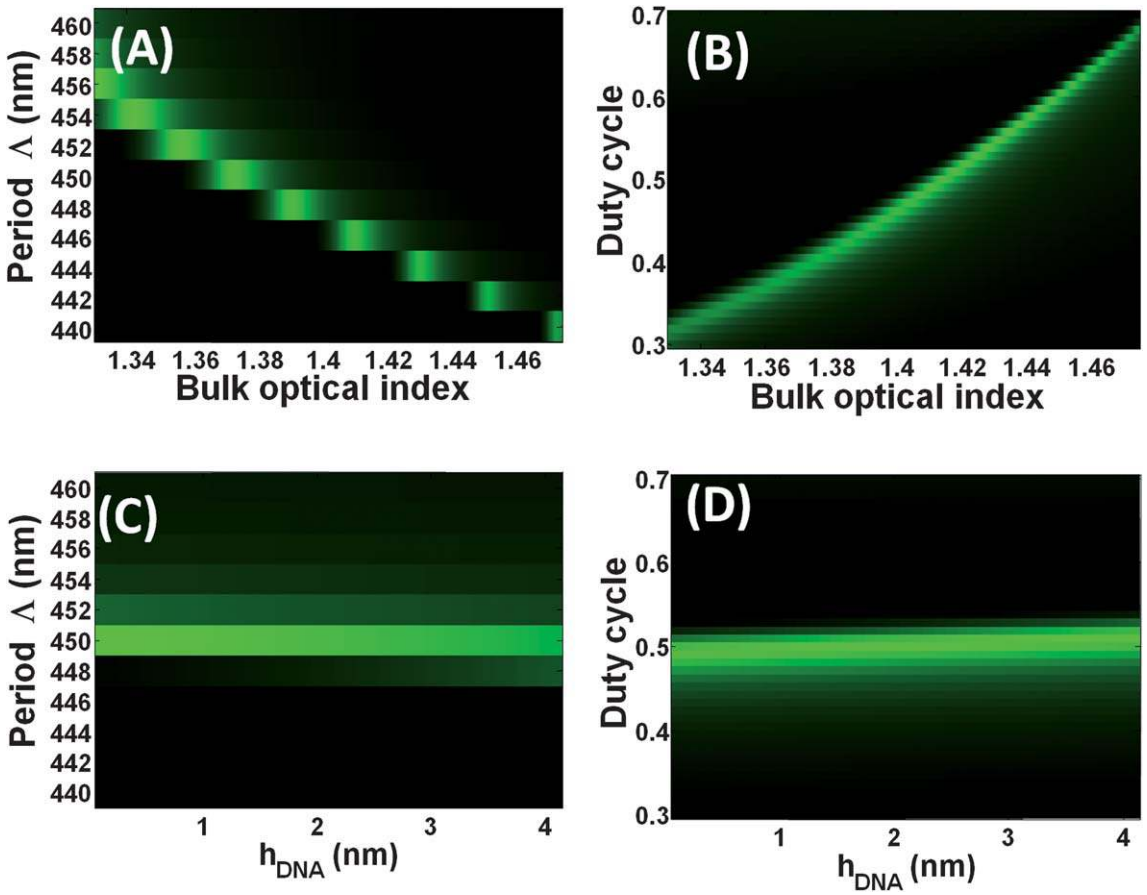

Fig. 2 Simulated diffraction efficiency reported on a [0 0.6] scale (A and B) for bulk index sensing with refractive index between 1.33 and 1.47, respectively with step of 1 nm for the line position (2 nm variation for period in the range [440–460 nm]), and for duty cycle variation by step of 4 nm for the groove width at fixed period $\Lambda_0 = 450$ nm (C and D) for biomolecules sensing modeled by thin layer of thickness h_{DNA} and optical index $n = 1.5$, identically for period variation and duty cycle variation.

variation (DV-PTC), or (C and D) depending on biological thickness on PV-PTC as well as DV-PTC. Fabrication limitations of micropads pattern of 1 nm in line position and 4 nm in groove width are taken into account in the modeling.

Refractive index sensing is studied on the range of refractive index [1.33–1.475] on PV-PTC and DV-PTC chips. As illustrated in Fig. 2(A), span of period in the range [440–460 nm] on our PV-PTC allows covering of the [1.33–1.475] refractive index range with good linearity. A change of refractive index $\Delta n = 0.1$ results in a shift of grating "micropad" of maximum diffraction efficiency by 5 "micropads" units ($\Delta\Lambda = 10$ nm difference in period). Due to the associated sparse sampling around the resonance, a fit realized with ~4 points results in RIU sensitivity accuracy of $\sim 10^{-2}$.

Fig. 2(B) gives the diffraction efficiency map on a DV-PTC chip, with a duty cycle varying in [0.3–0.7] stepwise $\Delta f = 4/450$ nm $= 0.00889$. Good linearity is obtained as well for refractive index sensing in the range [1.33–1.475]. In comparison to PV-PTC chip (Fig. 2(A)), it allows a much finer discretization in spite of the larger 4 nm feature-size step. Indeed, for the same change $\Delta n = 0.1$ the resonant point is shifted by 30 "micropads" ($\Delta d = 120$ nm, with d width of the groove, thus, $\Delta f = 0.267$). Therefore, a six-fold increase in precision is obtained when using duty-cycle rather than period variation. An index variation of $\Delta n = 10^{-5}$ therefore corresponds to a shift of 0.003 micropads, which can be detected with accurate fitting of the measured data, this accuracy being typically associated with a 3–5% accuracy in reflectivity of individual micropads, depending on the exact signal treatments.

Considering biological sensing, biomolecules are modeled as a thin layer of refractive index $n = 1.5$ and thickness h_{DNA} varying between 0 and 4 nm under an aqueous medium of constant index $n = 1.33$. The density of biomolecules at the chip surface in the case of partial coverage can further be modeled through the variation of the effective thickness of the biological layer. Dimensions of 1 to 4 nm are realistic considering biochip immunologic tests (typical size of protein 30 kDa) or DNA detection (average size of nucleotide 0.3 kDa with length typically from 20 to 200 bp). The shift caused by a bulk change $\Delta n = 10^{-5}$ results in the same change of reflectivity as a ~10 pg mm^{-2} layer (~modeled as a $h_{\mathrm{DNA}} \sim 0.015$ nm thin layer). Therefore, our technique allows sufficient sensitivity for label-free imaging of biomolecules hybridization.[8]

Note that although the expected sensitivities are already sufficient for most applications, an additional factor of × 4 in resonance profile sampling step should be possible. Indeed,

considering the machine-limited positioning precision in e-beam position of 1 nm (machine characteristics), some tricks in pattern design could be used to obtain an effective groove-width variation step of ~1 nm instead of 4 nm, thus increasing the sensitivity of the duty cycle variation tracks. An alternative method to obtain gratings micropads sampling a resonance condition would be to vary the waveguide layer thickness. From our diffraction efficiency calculation, a span similar to our current PTC is obtained for a 20% thickness variation of the guiding layer. Regarding fabrication issue, obtaining "micropads" of for instance 100 × 200 μm^2 areas each with constant but distinct guiding layer thicknesses would be very difficult to control by etching. A continuous gradient can be obtained by exploiting directionality in the deposition process[23] but it is however difficult to control and therefore may cause high disparity among the tracks if a M × N arrangement on the chip is foreseen. To finish this discussion, let us note that spanning a larger range of refractive index Δn is not *per se* a critical issue, as it may readily be obtained by extending "micropads" characteristics (for instance with a larger span of duty cycle, in combination with tracks of different period, use of TE polarization which is less dispersive, lower index guiding layer…).

Materials and methods

Imaging set-up

The chip is illuminated with high-power white LED from Thorlab, Inc (avoiding laser speckle). The beam is focused on the entrance slit of a SSM 301 monochromator from Zolix Instrument Co. Ltd. of Czerny–Turner configuration. The monochromator involves a grating of 1200 grooves mm^{-1} and has a focal length of 300 mm. The entrance and exit slits are adjusted to a width of 20 μm. A lens of focal length 150 mm then collimates the light from the exit slit, giving an angular resolution of 0.008°. The spectral width is of $\Delta\lambda \sim 0.2$ nm with these 20 μm slits. These limited angular and spectral spreads guarantee an almost negligible influence on our ~5 nm full-width at half maximum (FWHM) resonance response with a dispersion of 5.5 nm per degree. For these parameters, in order to exploit 90% of the camera dynamics, we use a 1 s integration time. The Canon EOS 5D camera is associated to a 65 mm focal length macro lens. The sample is placed on a 6-axis positioner for imaging. The 3 × 2 tracks PTC has dimensions 1.5 × 1.5 cm^2, which could be reduced in view of higher density sensing applications. Raw images are recorded by a Canon EOS 5D camera and are converted to 16 bits tiff format, giving a digitization precision of $\sim 2 \times 10^{-5}$. Each grating micropad is imaged on an area of ~400 pixels and we average over 5 successive images thus increasing the signal-to-noise ratio by a factor of $40 \sim (5 \times 400)^{1/2}$. Considering a typical relative noise of 4×10^{-3} on our CCD, the limit of detection is decreased to 1×10^{-4}.

Chip fabrication

The chip consists of borosilicate glass substrate ($n \sim 1.47$), covered by high-frequency PECVD silicon nitride layer ($P = 650$ mTor, Power 60 W, temperature of 300 °C, frequency 13.56 MHz using gas mixture SiH_4 40 sccm, NH_3: 40 sccm, N_2, 1800 sccm of index $n \sim 2.07 + 0.003i$ determined by ellipsometry measurement on a Si witness substrate. Nano-structuration is then realized using an electron-beam lithography process. Fig. 3 summarizes the successive steps of the process. The mask is laid out using L-Edit software. To prevent accumulation of charges from the electron beam on our dielectric chip, we first sputter 5 nm Cr layer on the support in a Cooke evaporation system (at $P = 5 \times 10^{-6}$ Torr, e-beam power source 3 kW. Photoresist ZEP-7000 is spin-coated at 2000 rpm and backed for 1 min at 180 °C prior to exposure. Exposure is realized with a JEOL JBX-6300FS e-beam system using high-precision mode to vary the groove width by step of 4, with a 100 kV energy, 1 nA current and dose 50 mC cm^{-2}. The photoresist is then developed with ZEP500 developer. The uncovered part of chromium is etched away by reactive ion etching process using an AST Cirie 200 machine ($P = 10$ mTorr, power 300 W, Cl_2 45 sccm for 120 s. The SiN layer is then etched on 50 nm thickness with an AME8110 RIE according to an established process ($P = 50$ mTorr, power 1200 W, and a gas mixture of CH_4 74 sscm and O_2 6 sccm for 5 min. The remaining photoresist is then stripped by O_2 plasma process for 20 min at 100 °C temperature in O_2 Asher. The remaining chromium is finally etched away using RIE again.

As chromium etching has low selectivity towards the photoresist layer, scanning electron microscopy (SEM) characterization is realized after each etching step. From our SEM measurement after process completion, for the period $\Lambda_0 = 450$ nm, the groove width targeted to vary from 140 nm to 310 nm actually varies from 71.6 nm to 292.23 nm, thus achieving a duty cycle range between 0.159 and 0.650. Therefore, we model the groove width error d_e by a fitted logarithmic law $d_e = -14 \times \log(\text{grating number}) + 69.382$. This same groove width error is employed for the period variation pattern, which for the central period Λ_0 corresponds to $f \sim 0.443$.

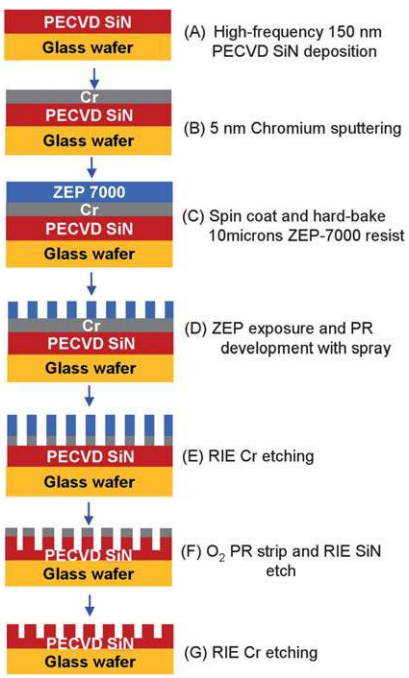

Fig. 3 Process flow of RWG PTC device as indicated (A–G).

Image analysis

Acquired images are recorded in raw format and further converted in 16 bits images. To reduce noise contribution, 5 successive images are recorded and further averaged. The obtained RGB image is converted in intensity color by averaging the 3 components. The profiles are then realized using ImageJ and Matlab, by localizing the pixels corresponding to a given micropad. Sequence over the micropads is then obtained for each track, and used to determine the micropad of maximum diffraction efficiency equivalent position. The refractive index of bulk solution or biological layer equivalent thickness can be deduced from this maximum position.

Bulk sensing

Our first demonstration of a PTC demonstrates bulk liquid sensing. To apply different refractive indices at the chip surface, we fabricate a structure with separate chambers, each associated to a single track, and where fluids of different refractive indices can be introduced. To limit background stray light from the fluidic parts, we chose a carbon-PDMS (polydimethylsiloxane) material. PDMS is prepared with Sylgard 184 (Dow Corning) silicone elastomer mixture, a two-part heat curable system that is mixed at a weight ratio base : curing agent : carbon powder 10 : 1 : 1 (w/w/w). To form the chambers, we made PDMS molds with chambers defined by a soft lithography process. The chambers dimensions are 1.5 mm × 5 mm with a height of 100 μm. The C-PDMS chambers are baked for 2 hours at 60 °C. Different bulk solutions are then injected in the chambers prior to imaging as illustrated in Fig. 4(A). PTC chip format is of 3 × 2 tracks and 6 media can be sensed in parallel in a single image frame. The refractive indices vary between 1.333 and 1.474 by using water–glycerol solution, with composition 100 : 0, 80 : 20, 60 : 40, 40 : 60, 20 : 80, 0 : 100 to get a linear refractive index variation with a $\Delta n = 0.028$ step. Fig. 4(B) reports the acquired tracks image for a PV-PTC chip with gratings of different periods along tracks, and Fig. 4(C) reports the acquired tracks image for a DV-PTC chip with different duty cycles along tracks. A red arrow on each track indicates the reference position. This contribution is taken into account in the analysis as will be discussed further in the following. Experimental profiles are then realized from these images, clipping ~20 × 20 centered pixels in each micropad.

In Fig. 5 , (A and B) we give simulated profiles for our structure as well as (C and D) experimental profiles realized from the images given in Fig. 4. Fig. 5(A) shows the simulated profile of our PV-PTC for different bulk medium. To show the discretization, we represent the micropad expected signal with circles on the continuous profile. Similarly, in Fig. 5(B) we give the simulated tracks profiles as a function of the duty cycle, and represent by circles expected signal for each micropad. Experimental profiles are reported in Fig. 5(C) for the PV-PTC chip and Fig. 5(D) for the DV-PTC chip. Both due to inhomogeneities of the fabricated structure (mainly variation of the guiding layer thickness), as well as optical settings, we first realize a reference image using water as ambient medium. Position of the maxima of this reference image are indicated by arrows on Fig. 4(B) and (C). Green profiles correspond to the measured profiles from images

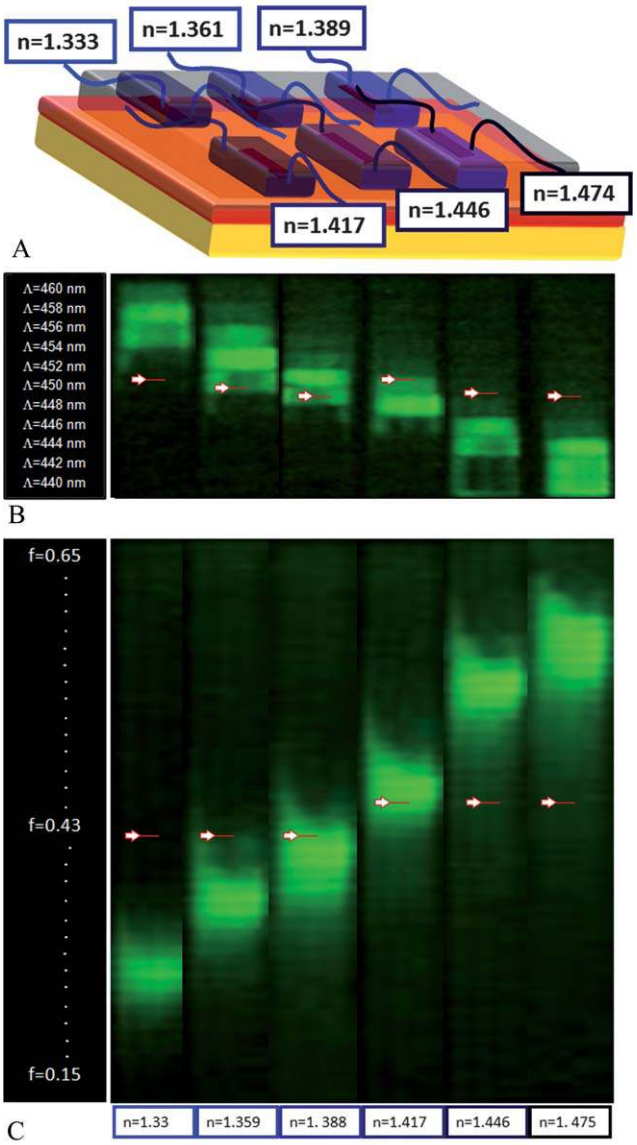

Fig. 4 (A) Scheme of the multiplex chip with different chambers in which bulk solution of 6 different refractive indices (from 1.33 to 1.47, with linearly varied water/glycerol fractions). (B) Tracks images extracted from a single 3 × 2 PTC image for different period gratings. (C) Tracks images extracted from a single 3 × 2 PTC image for different duty cycles gratings. Micropad dimensions are 90 μm × 200 μm with 10 μm separation and image is therefore flattened for convenient representation. A red arrow indicates the "reference position" to account contribution from tracks differences and optical settings.

shown in Fig. 4. To account for the variable reference position of each track, we translate the experimental profiles by a given number of units, possibly fractional since it comes from the fitted reference data. The resulting profiles are presented in blue color. Experimental measurement shows dispersion generally lower that those expected from theory. This might be due to higher losses from imperfection of the surface or from a spatially variable silicon nitride optical index. This weaker dispersion is taken into account in the modeling by the addition of a 40 nm layer of

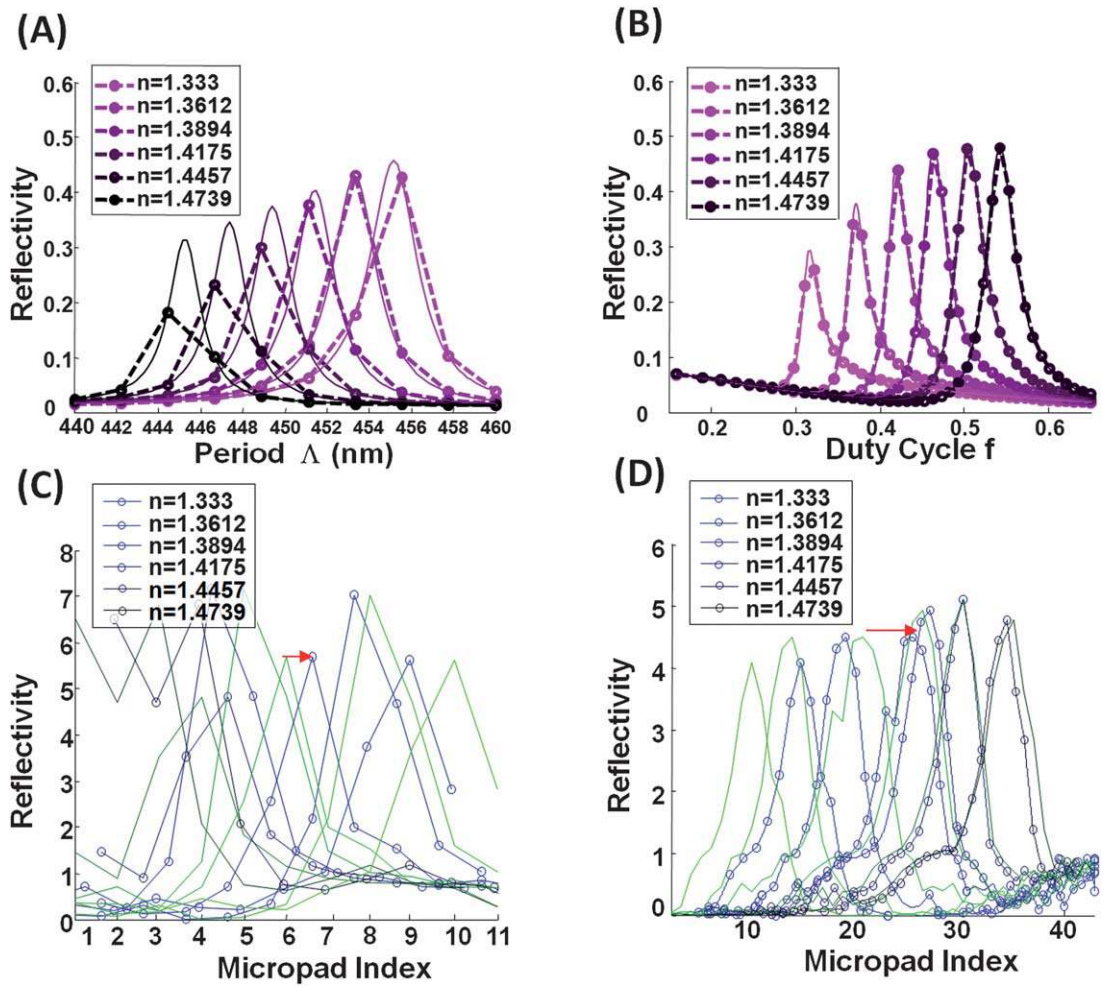

Fig. 5 (A) Simulated reflectivity profiles for bulk reflective index sensing for 6 different water–glycerol solutions with index varying linearly between 1.333 and 1.474, for varying period (PV-PTC). The dotted line with circles indicates points corresponding to each micropad (B) simulated reflectivity profiles for bulk reflective index sensing with varying duty cycle (DV-PTC). The dotted line with circles indicates points corresponding to each micropad. The fabricated duty-cycle "error" d_e (see text) is taken into account in the modeling (C) experimental values on PV-PTC tracks for different bulk medium. Green lines going through data at integer micropad number correspond to raw experimental data, while the blue lines with circles are corrected by a non-integer micropad number difference obtained from the reference image measurement A red arrow underlines an example. (D) Experimental values on DV-PTC tracks for different bulk medium. As in (C), green lines are raw data, blue ones include the correction obtained from the reference image measurement (*cf.* red arrow).

effective index 1.5 over the grating. We remind that the modeling takes into account the smaller groove width in comparison to the targeted value. Our silicon nitride layer is estimated to be 0.33Λ instead of 0.27Λ. For accurate measurements in applications, tracks dispersion will have to be calibrated prior to chip use, although a higher accuracy should readily result from better technology and dry assessments.

We first discuss the shift obtained for tracks with period variation through their micropads. From the software limitation of our e-beam system, the written stripe groove width is multiple of 4 nm while the period can evolve more smoothly, which implies a small adjustment of the filling factor. As a line width smaller than the target values by 25 nm than targeted has been determined, the corresponding duty cycles vary around $\sim 0.443 \pm 0.004$ instead of 0.500. The precision obtained from the current period variation track exploitation is limited to a $\Delta n \sim 10^{-2}$ accuracy (troubles in fit linearity), which would correspond to 10 ng mm^{-2} precision for biology application and is insufficient for microarray applications. We suspect that limitations similar to the one encountered here may have prevented the accurate exploitation of grating-based approaches in various areas. Let us nevertheless discuss the limits assuming that such issues can be solved.

As is seen before; the DV-PTC allows 6 times more points to be obtained than the PV-PTC for a given optical index variation, Δn. It renders fitting much more accurate and leads to much better sensitivity concerning index detection variation. Fitting the sampled profiles with Lorentzian curves for analyzing these tracks profiles, we get a detection limit of $\Delta R = 1 \times 10^{-4}$ in terms of equivalent reflectivity variation at a single angle, that corresponds to a detection limit 2×10^{-6} of RIU from numerical simulation. Therefore, a sensitivity of $\Delta n = 10^{-5}$ is suitable for most applications, and seems a very realistic expectation for our detection technique when including potential contributions for

improved accuracy analysis (fabrication variability, optical settings, fitting approximations…). For biological applications, such accuracy typically corresponds to a density of ~10 pg mm^{-2} in aqueous medium.[11] To get higher sensitivity, our biological demonstration with hybridization and immobilized molecules rather emphasizes the duty cycle chip, described as follows.

Biological sensing

To assess biological layer sensing with our "peak-tracking chip", we test the quantitative aspect and detection sensitivity of our technique through hybridization reactions with different concentrations of DNA molecules. Probes are first immobilized on the whole chip. Considering the silicon nitride layer is actually $Si_xN_yO_z$ with sufficient oxygen density to allow DNA immobilization (with surface occupancy consideration of maximum 3 × 3 nm^2 per DNA probe), we choose an hydroxyl based functionalization as follows. The chip is first cleaned through O_2 plasma, before 10 min NaOH bath at 10^{-1} M concentration. All bath cleaning steps are realized with rotation of 100 rpm (or ultrasonics when specified). The chip is then cleaned for 5 min in successive baths of ethanol, ethanol/water 97.5 : 2.5, ethanol/water 95 : 5. It is then put for 2 hours in 1% APTES (amino-propyl-tri-ethoxy silane) solution in ethanol/water 95 : 5 solvent. It is then cleaned for 10 min in ethanol/water 95 : 5, then ethanol/water, 10 min ethanol/water 97.5 : 2.5 with rotation shaking, and finally 15 min ethanol with ultrasonics, before 15 min baking at 100 deg. The chip is then incubated overnight with probes at 5 μM concentration in 3× SSC buffer, with 1.5 M betaine, and rinsed for 2 minutes in the successive solution 1× SSC (saline-sodium citrate), 0.2% SDS (sodium dodecyl sulfate), 0.1× SSC, 0.2% SDS, and finally 0.1× SSC. To study the quantitative aspect of hybridization reaction, we realize a fluidic structure with individual chambers for each track. These hybridization chambers have dimensions of 2 × 5 × 2 mm^3 corresponding to a volume of 20 μL. The fluidic structure is first passivated with 0.1%m BSA in 4× SSC, 4% isopropanol. The target is then introduced in the different chambers in a hybridization buffer composed of 5× SSC, 0.1% SDS, 25% formamide, H_2O. The probe and target are ordered from Invitrogen. The probe sequence is the following 5′-TTTTTTTTTTCGCCAGA TACCGTGCTAG-3′. The introduced target is of 100 base pairs of sequence 3′-GCGGTCTATGACACGATCGTCCGCATGG CGCAGCCATTCTCGCTGCGTTATATGCTGGTAGACGG TCAGGGTAACTTCGGTTCTATCGACGGCGACTCTG-5′ with Cy2 label (we chose a fluorescently labeled target in order to perform control experiments). It was chosen in view of future studies of single nucleotide polymorphism in the framework of resistance to the antibiotic ciprofloxacin.[24] This 100-base-pairs DNA fragment (with gyrase A sequence from *E. coli* K12 genome) has a 30.8 kDa molecular weight and is appropriate to illustrate the compatibility of our technique either with immunoassays or DNA assays using pre-amplified PCR (polymerase chain reaction) DNA fragment. Further integration of our chip based detection technique with PCR step on the same chip support, thus leads to a compact system for *E. coli* population analysis as well as to extend our PTC into a whole integrated analysis system[25,26] which may also facilitate biological applications for real biological samples.

The target concentrations introduced in the different 20 μL chambers are the following: 2 nM, 5 nM, 10 nM, 25 nM, 100 nM, and we waited for 2 hours to obtain the hybridization reaction. The chip was then rinsed using the same process as after probes immobilization. In order to be able to compare the quantity of bio-molecules on each of the pads without being affected by fabrication variability across pads, we compare the obtained PTC image to a reference image made before any biological step. In view of real-time hybridization detection, we realize this measurement in aqueous buffer solution. The contrast is then lower than the one that could be obtained in air for end-point detection, but validates the compatibility of our technique for real-time analysis. To robustly quantify the amount of biomolecules hybridized at the chip surface, we realize some control fluorescence measurement. They were performed using the Typhoon 3 system from General Electric. Fluorophores are excited at a wavelength of 488 nm to excite the Cy2 label, and imaged at 550 nm with a pixel resolution of 25 μm, thus providing knowledge of the density on each micropad. Next, reflectivity images similar to those for bulk index sensing are realized, and analyzed to determine the amount of biomolecules on the chip surface calculated by measuring the shift in the reflected intensity profile along each of the tracks, which is naturally given in micropad units. The maximum measured shift is of 0.43 micropads with accuracy 0.04 micropads, which for our fabricated chip would correspond to a 1.6 nm layer, and is consistent with our expectation of a monolayer of 100 bp DNA. The saturation is obtained with a concentration of 10 nM. Considering the introduced volume of 20 μL and a pad surface of 10 mm^2, the corresponding calculated density is of 2.4 × 10^{12} molecule per cm^2 or equivalently 1.22 ng mm^{-2} for our 30.8 kDa 100 bp molecule. As a determination of the surface mass density for the lower concentration experiments, *i.e.* to account for variations in surface density, we normalize the fluorescence signal on each track by the fluorescence signal corresponding to the maximal density. A plot of the shift *vs.* surface mass density extracted with these precautions is reported in Fig. 6.

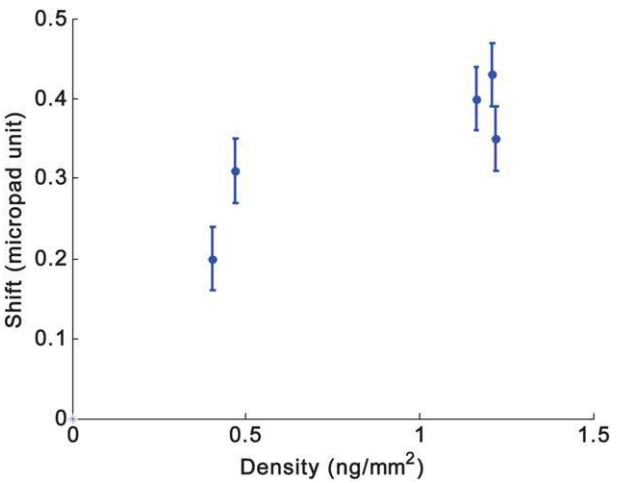

Fig. 6 Measured shift in micropad unit for DNA sensing application with error bars of 0.04 units. Fluorescent control signals are converted in surface densities assuming the maximal density (*i.e.*, maximum fluorescent signal) of 1.22 ng mm^{-2}.

Inhomogeneous binding over the whole track still results in approximations on the peak position. But the simple fact that we can retrieve substantial accuracy in spite of relatively adverse conditions at the single-micropad level shows that our procedure is much more robust than single-grating ones. Furthermore, a potential improvement would be the stabilization of the fluidic structure so the chip can be left in the same position on the optical set-up while introducing the biological sample.

Note that large tracks with as much as 43 units have been presented, in order to cover the whole range of refractive index [1.33–1.475]. Changes induced by biological thin layer occur on a much smaller range (~maximum 2 micropad units). A duty cycle range in [0.45–0.55] (corresponding to 11 micropads for $\Delta f = 0.0089$) should fulfil the conditions of sufficient domain for good fitting as well as accurate coverage for the expected shift and potentially accounting tracks different reference position, thus allowing to increase N × M track density in the hundreds. A higher density of tracks might also be obtained by optimizing their shape through different positioning or dimension of the micropads.

Multi-spectral imaging with pre-dispersed illumination

In addition to multiplex sensing property, another promising aspect of our chip is to design tracks of different optical properties on the same chip support, for instance to sense different wavelengths or different polarizations in parallel. Such multifunctional tracks may for instance be used (i) to determine a refraction law (dispersion) over the visible domain [400–650 nm]: tracks would then have central periods from $\Lambda = 330$ to $\Lambda = 534$ nm, or (ii) to study *e.g.* liquid crystals with polarization-dependent anisotropic optical index, or similarly for polarization rotating compounds. For fabrication purpose, rescaling the waveguide layer thickness by a factor $\Lambda/\Lambda_{450\text{nm}}$, here in the range 0.84–1.36, separately on each micropad, is clearly delicate. However, very reasonable sensitivities can still be obtained without any rescaling, *i.e.* with constant thickness. Whole-visible-spectrum sensing can be used for simple characterization of an optical medium, or to study broadband properties of biomolecules.[26,27] In addition to biochemical applications, characterization of liquid medium optical index is of high interest in the field of optofluidic, as a simple characterization tool.[28] Such colorimetric assessments can be obtain through series of monochrome images of tracks on single PTC, or most importantly on a single image of our PTC but using predispersed illumination (linking angle and wavelength, obtained for instance using prism or grating), so each track is illuminated with quasi-monochromatic light. Concerning the polarization, to excite the TE resonance using same incidence condition as in the TM case presented in this paper, the grating period has to be decreased to $\Lambda \sim 400$ nm. If the main modified parameter is the central period of the "pads", the phase-matching condition can still be satisfied on a relatively small incident angle interval. Furthermore, in a N × 2 geometry, both whole spectrum as well as polarization might be obtained using the same PTCimage information. Concerning polarization, TE and TM contributions can be separated through the optical set-up or by subtracting the non-resonant contribution on track images. Due to our PTC property of spanning range of neighboring conditions on each of its tracks, fabrication variability from design is safely corrected and ensures one of the track micropad corresponds to resonance peak. Therefore, these multispectral and multipolarization aspects would increase further the interest in our PTC approach to measure broadband dispersion law of the materials.

Conclusion

In this paper, we have presented a new refractive index sensing method, based on profile measurement obtained through a simple camera image under monochromatic collimated incoherent TM illumination. Our general principle is to "fold" the resonance tracking dimension generally needed in resonant measurement optical techniques into the imaging procedure itself, since the very high throughput of images, tens of megapixels, still leaves ample margin for multiplexing biologically tens or maybe hundreds of reactions. Specifically, spectral profiles of most-developed RWGs multiplex techniques are replaced by spatial profiles through "tracks" structures on the chip surface. These "tracks" have geometry designed to scan the resonance profile by slowly varying the parameter the most successful of which was found to be the duty cycle. Our "peak tracking chip" technique is shown to perform well in term of sensitivity, and to achieve its scope of being robust to optical background or positioning contributions. Reference "tracks" can also serve to control and disentangle slight mechanical motions of the sample, or in the case of bio-detection application, fluidic refractive index changes induced by temperature drift or nonspecific biological binding.

Through a carefully controlled and characterized process, we realized multiplex sensing experiments, first to validate bulk sensing application, and then to validate biological sensing in microarray format. For this purpose, we fabricated a 3 × 2 "tracks" PTC on silicon nitride waveguide with glass support for visible imaging ($\lambda = 547$ nm). Tracks with varying duty cycle units of period $\Lambda = 450$ nm and duty cycle variation $\Delta f = \delta/\Lambda = 0.0089$ between neighboring units allow 6-fold finer discretization than for the period variation by step of 2 nm between 440 nm and 460 nm (steps limited by the fabrication). Our bulk optical index sensing experiments carried out with solution between $n = 1.333$ and $n = 1.474$ demonstrated good linearity as well as good agreement with predicted results.

Quantitative detection of immobilized ~30.8 kDa molecules was presented in aqueous medium with mass coverage between 0.2 and 1.2 ng mm^{-2}, corresponding to a bulk sensitivity of 2×10^{-4} RIU. From measured data, this seems the limit of obtainable sensitivity when moving the chip from and to the set-up and using reference track. With a noise contribution $\Delta R \sim 1 \times 10^{-4}$, a theoretical sensitivity of 2×10^{-6} RIU should be possible. Taking into account our combined experimental results and simulations, a practical sensitivity of 10^{-5} RIU (~10 pg mm^{-2}) seems a reasonable expectation for our novel PTC based technique, corresponding to a ~10 pg mm^{-2} for protein or DNA sensing. Although with the present process, the chip might be used several times by performing O_2 plasma cleaning, though in successive experiments, the chip may encounter damage in its surface quality/structuration. Therefore, in view of large number of chips fabrication and cost reduction, the electron beam lithography process shall be replaced by a nanoimprint process, where good control of nanopattern at few nm range was

demonstrated.[30] To increase uniformity between different areas of the chip, processes such as atomic layer deposition could be used for the waveguide layer. Although the chip readily features decent sensitivity, a further increase might be obtained through decreasing the current 4 nm groove width interval (through different pattern writing strategies or using the dose (e-beam current)). Several geometry parameters might also be varied at the same time, the easiest to vary for identical tracks in 2D geometry being period and duty cycle.

By definition of the "on-chip" system, our system is compact. Considering pads dimensions (typically 0.2×4.3 mm^2 for DV-PTC with duty cycle [0.3–0.7] and height of the chamber of 1 μm (vertical extent of the wave being less than few hundred nm), sensing of droplets of less than one nanoliter can be implemented.[29] Chip functions may also be diversified by implementation of temperature control (then replacing C-PDMS by black-anodized aluminum) for temperature dependence of refractive index depending studies.

Interest of multiplex detection technique with the use of cheap set-up (simple camera detector) and monochromatic/quasi-monochromatic polarized light is no longer to be demonstrated as stated by the success of SPR imaging technique. Together with RWGs flexibility advantages, we foresee a large range of biological applications of our PTC. Together with multiple characteristics tracks on a single chip, powerful variants of our chip functions are expected to open new research directions, notably for spectroscopy and index anisotropy.

Other 2D or 3D dielectric photonic structures than RWGs can be foreseen, potentially increasing further the sensitivity. We note that in principle, the idea of tracking properties around the resonance could also be applied to nano/micro-structured chips with surface plasmon resonance properties.[31]

Acknowledgements

The project is supported by HKUST Special research fund initiative SRFIEG01 and RGC grant number 604710. The electron beam lithography project is supported by Hong-Kong government under the project SEG HKUST 10. The authors are grateful to HKUST nanofabrication facilities staff for their help in the chip fabrication process, and more particularly to K. C. Li Nelson and M. W. Lee Preason for their high quality work for well-controlled process. We thank as well Robert H. Austin and Yuen Ron Shen for fruitful discussion and Xiaoteng Luo and Rimantas Kodzius for experimental advice.

Notes and references

1 A. L. Washburn and R. C. Bailey, *Analyst*, 2011, **136**, 227–236.
2 X. Fanand and I. M. White, *Nat. Photonics*, 2011, **5**, 591–597.
3 X. Fang, C. Liu, X. Cheng, Y. Wangand and Y. Yang, *Sens. Actuators, B*, 2011, **156**(2), 760–764.
4 H. Choumane, N. Ha, C. Nelep, A. Chardon, G. O. Reymond, C. Goutel, G. Cerovic, F. Vallet, C. Weisbuch and H. Benisty, *Appl. Phys. Lett.*, 2005, **87**(3), 031102.
5 N. Ganesh, W. Zhang, P. C. Mathias and B. T. Cunningham, *Nat. Nanotechnol.*, 2007, **2**(8), 515–520.
6 E. L. Moal, S. Leveque-Fort, M. C. Pottier and E. Fort, *Nanotechnology*, 2009, **20**, 225502.
7 K. Ray, M. H. Chowdhury, J. Zhang, Y. Fu, H. Szmacinski, K. Nowaczyk and J. R. Lakowicz, *Adv. Biochem. Eng./Biotechnol.*, 2008, **16**, 1–28.
8 M. Piliarikand and J. Homola, *Sens. Actuators, B*, 2008, **134**(2), 353–355.
9 E. M. Yeatman, *Biosens. Bioelectron.*, 1996, **11**, 635–649.
10 O. Parriaux and P. Sixt, *Sens. Actuators, B*, 1995, **29**(1–3), 289–292.
11 M. Wikiand and R. E. Kunz, *Opt. Lett.*, 2000, **25**(7), 463–465.
12 D. Bhatta, A. A. Michel, M. Marti Villalba, G. D. Emmerson, I. J. D. Sparrow, E. A. Perkins, R. W. Ely and G. A. Cartwright, *Biosens. Bioelectron.*, 2011, **30**(1), 78–86.
13 K. Bougot-Robin, J. L. Reverchon, M. Fromant, L. Mugherli, P. Plateau and H. Benisty, *Opt. Express*, 2010, **18**, 11472–11482.
14 P. Li, B. Lin, J. Gerstenmaier and B. T. Cunningham, *Sens. Actuators, B*, 2004, **99**(1), 6–13.
15 A. M. Ferrie, Q. Wu and Y. Fang, *Appl. Phys. Lett.*, 2010, **97**(22), 223704.
16 S. George, I. D. Block, S. I. Jones, P. C. Mathias, V. Chaudhery, P. Vuttipittayamongkol, H. Y. Wu, L. O. Vodkin and B. T. Cunningham, *Anal. Chem.*, 2010, **82**(20), 8551–8557.
17 J. Dübendorfer and R. E. Kunz, *Sens. Actuators, B*, 1997, **38**(1–3), 116–121.
18 L. Li, *J. Opt. Soc. Am. A*, 1996, **13**(5), 1024–1035.
19 S. G. Tikhodeev, A. L. Yablonskii, E. A. Muljarov, N. A. Gippius and T. Ishihara, *Phys. Rev. B: Condens. Matter Mater. Phys.*, 2002, **66**(4), 045102.
20 A. David, H. Benisty and C. Weisbuch, *Phys. Rev. B: Condens. Matter Mater. Phys.*, 2006, **73**, 075107.
21 L. Martinelli, H. Benisty, O. Drisse, E. Derouin, F. Pommereau, O. Legouézigou and G. H. Duan, *IEEE Photonics Technol. Lett.*, 2007, **19**, 282–284.
22 R. J. Bojko, J. Li, L. He, T. Baehr-Jones, M. Hochberg and Y. Aida, *J. Vac. Sci. Technol., B: Nanotechnol. Microelectron.: Mater., Process., Meas., Phenom.*, 2011, **29**(6), 06F309.
23 N. Ganesh, A. Xiang, N. B. Beltran, D. W. Dobbs and B. T. Cunningham, *Appl. Phys. Lett.*, 2007, **90**(8), 1063.
24 Q. Zhang, G. Lambert, D. Liao, H. Kim, K. Bougot-Robin, C. K. Tung, N. Pourmand and R. H. Austin, *Science*, 2011, **333**(6050), 1764–1767.
25 J. Wu, W. Cao, W. Wen, D. C. Chang and P. Sheng, *Biomicrofluidic*, 2009, **3**(1), 012005.
26 J. Wu, R. Kodzius, K. Xiao, J. Qin and W. Wen, *Biomed. Microdevices*, 2012, **14**, 179–186.
27 J. T. Bradshaw, S. B. Mendes and S. S. Saavedra, *Anal. Chem.*, 2005, **77**(1), 28–36.
28 B. M. Beam, R. C. Shallcross, J. Jang, N. R. Armstrong and S. B. Mendes, *Appl. Spectrosc.*, 2007, **61**(6), 585–592.
29 K. S. Chao, T. Y. Lin and R. J. Yang, *Microfluid. Nanofluid.*, 2012, **12**(5), 697–704.
30 H. J. Park, M. G. Kang and L. J. Guo, *ACS Nano*, 2009, **3**(9), 2601–2608.
31 T. Y. Chang, M. Huang, A. A. Yanik, H. Y. Tsai, P. Shi, S. Aksu, Y. M. Fatih and H. Altug, *Lab Chip*, 2011, **21**, 3596–3602.